AIMS Electronics and Electrical Engineering

http://www.aimspress.com/journal/ElectrEng

AIMS Electronics and Electrical Engineering, 7(3): 196–216.
DOI: 10.3934/electreng.2023012
Received: 27 May 2023
Revised: 17 July 2023
Accepted: 03 August 2023
Published: 09 August 2023

Research article

Enhancing sensor linearity through the translinear circuit implementation of piecewise and neural network models

Seenivasaan Sundararajan*and Madhusoodanan Kottarthil Naduvil

Department of Instrumentation, Cochin University of Science and Technology, Cochin, Kerala, India

* **Correspondence:** Email: sunda.79@gmail.com; Tel: 9846922914.

Abstract: The performance of the control system relies on the linearity of the sensor, which can be influenced by various factors such as aging and alterations in material properties. However, current sensor linearization techniques, such as utilizing neural networks and piecewise regression models in the digital domain, suffer from issues like errors, excessive power consumption, and slow response times. To address these constraints, this investigation employs a translinear based analog circuit to realize neural networks and piecewise regression models for the purpose of linearizing the selected sensors. A conventional feed-forward back propagation network is constructed and trained using the Levenberg-Marquardt algorithm. The developed linearization algorithm is implemented using a translinear circuit, where the trained weights, biases, and sensor output are fed as input current sources into the current-mode circuit. Further in this work, the piecewise regression model is designed and implemented using a translinear circuit and the breakpoint is determined using 'R' language. The simulation results indicate that the implementation of the current-mode circuit with metal-oxide-semiconductor field-effect transistors (MOSFETs) for the neural network algorithm leads to a substantial reduction in full-scale error as compared to the piecewise current mode model. Additionally, a performance analysis was conducted to compare the utilization of current-mode circuits with digital approaches for the linearization of sensors. The proposed translinear implementation surpasses the other researcher's work by delivering notable results. It showcases a significant improvement in linearity, ranging from 60% to 80%, for the selected sensors. Furthermore, the proposed implementation excels not only in linearity but also in terms of both response speed and power consumption. The improvement in the linearity of the sensor can be enhanced further by replacing the MOSFETs with bipolar transistors or any versatile materials such as gallium arsenide or gallium nitride-based transistors.

Keywords: sensor; linearization; neural network; translinear circuit; power consumption

1. Introduction

Sensors play a crucial role in various industries including automotive, electronics, mining, and waste management. The properties of a sensor directly impact important parameters such as process productivity, resilience and accuracy, particularly within the automation industry. However, the nonlinearity of sensors, influenced by factors like the properties of the metallic components, aging effects and hysteresis errors, imposes limitations on the performance of processes in automation. In the literature, numerous methods for linearization have been proposed, categorized as either hardware-based or software-based approaches.

Thermocouples hold significant importance within the manufacturing industry, primarily employed for temperature measurement in furnaces and molten metal applications. The nonlinearity errors observed in thermocouples stem from two major factors: the cold junction temperature and the properties of the metal, specifically the Seebeck coefficients. The hardware circuit, as described in reference [1], processes the output signal from the thermocouple using a voltage-controlled oscillator (VCO). The resulting signal is then transmitted to a PC for further processing, where a suitable algorithm is employed to extract the cold junction temperature. Utilizing a two-dimensional continued-fraction-based algorithm, the hot junction temperature is accurately measured while minimizing non-linearity within a range of ±1.4°C. The proposed hardware plus software-based approach in the study [2] employs the inverse reference function for linearizing the K-type thermocouple in the range of -100°C to 1372°C. A decent improvement in the linearity of ±1°C is obtained by referring to the thermo-emf vs temperature reference table. A dual input logarithmic amplifier is proposed in the work [3] to linearize the T-type thermocouple in the range of 0-100°C. Appropriately choosing the value of λ which is the ratio of feedback resistance to the bridge resistance can improve the linearity. The normalized linearity error of 0.0018 is achieved in the work [3]. The logarithmic amplifier built with the ratiometric function is proposed in the work by the investigators [4] to linearize the various types of thermocouples. The linearity improvement in terms of less root mean square error of 0.051 is achieved for T-type thermocouple over the temperature range of 0-400°C. The optimal local linear models are used via a data-driven approach to linearize various thermocouples, as discussed in the paper [5]. Excellent improvement in the linearity of ±0.12% and ±0.41% is achieved for J-type, and K-type thermocouple is achieved in the proposed multi-linear model approach [5]. To linearize the thermocouple, the authors [6] use a radial basis function-based neural network technique with a gradient descent algorithm for tuning its parameters. Despite implementation problems, the work [6] addresses a significant amount of linearity improvement. The MOSFET-based translinear circuit for realizing the non-linear function to linearize the T-type thermocouple is proposed in the work [7]. A decent improvement in the linearity of 75% is reported with less power consumption.

The Pt100 sensor, which has a resistance of 100Ω at 0°C (32°F), is the most prevalent sensor in the process industry. The error between the temperature and the resistance curve is substantially high in the low-temperature region (from 50°K to 200°K) and small in the high-temperature region. One of the methods proposed in the literature [8] employs the analog circuit with a positive feedback path with calibration performed as transfer function fragmentation yields better results. The bridge circuit-based linearization of RTD is proposed in the literature [9]. The circuit is built with the transfer function of RTD with an absolute error term introduced and the error is reduced with the aid of a bridge circuit, differential amplifier, and supply voltage former. A decent amount of linearity of 0.1°C is reported

in the work [9]. The logarithmic ratiometric function with its parameters is optimized using the evolutionary algorithm employed for linearizing the RTD proposed in the work [10]. The LABVIEW-based implementation [10] of non-linear function completely eliminates the problem of the non-linearity of any sensor. The linearization of RTD with a voltage divider and feedback compensation is proposed [11] with the estimated error after linearization being 0.5°C.

The implementation of two-stage piecewise linearization proposed in the work [12] for the linearization of thermocouples results in a better reduction of error. The study [13] reports a non-linear regression approach for K-type thermocouples with good linearity of 0.02%. The polynomial estimation method of linearizing T-type thermocouple, discussed in the work [14], results in an accuracy of 0.3°C. In the study referenced as [15], Artificial Neural Networks (ANN) are suggested as a linearization technique, demonstrating effective linearity through inverse modeling. However, challenges related to implementation have been encountered.

In this study, the application of piecewise and neural network regression models through the analog mode circuit (Translinear) is introduced to achieve linearization of thermocouples and RTDs. The effectiveness of the linearization approach is assessed by quantifying the full-scale error (FSE). The research [16] introduces an approach that utilizes translinear circuitry to implement an evolutionary optimized non-linear function, specifically for the purpose of linearizing different thermocouples. This work serves as a notable reference point for comparing the results of the proposed translinear implementation.

2. Materials and method

2.1. Piecewise regression

Piecewise regression, also referred to as segmented regression or broken-stick regression, is a regression analysis method that divides the independent variable into intervals and fits each interval with a separate line segment. It is particularly useful for modeling data that exhibits a change point or breakpoint. The precise location within the variable where the functional form changes plays a crucial role in segmented regression, as it signifies a shift in the data pattern. This shift is typically represented by a node, a shared point, or a change point. In this study, the parameterization of segmented linearization is defined as follows.

$$f(x) = \begin{cases} \beta_0 + \beta_1 \times x, & \text{if } x \leq \gamma. \\ \beta_0 + \beta_1 \times x + \beta_2 \times (x - \gamma), & \text{if } x > \gamma. \end{cases} \tag{2.1}$$

where β_0 is the y intercept, β_1 and β_2 are the regression coefficients and γ is the break point.

2.2. Neural network

Artificial neural networks (ANN) are a form of machine learning that leverages artificial intelligence to identify patterns within extensive datasets. They are capable of predicting outputs based on given inputs using either neural networks or linear regression models. The effectiveness of regression models relies heavily on the suitability of the regression equation for the data at hand. Despite their computational complexity, neural networks possess versatility as they can dynamically adapt and select the most suitable regression approach. The process of linearizing a sensor can be perceived as a regression problem, aiming to forecast sensor output by utilizing target or straight-line data.

2.2.1. Levenberg-Marquardt algorithm

A widely used technique for training a linear regression problem is the back-propagation algorithm, which employs the gradient descent method (GD) in a supervised learning setting. Its objective is to minimize the network's error by propagating the gradient of the error curve, as described in reference [17]. To achieve error function minimization, the back-propagation algorithm utilizes the Levenberg-Marquardt (LM) algorithm, where a conservative step size is maintained to ensure the accuracy of the linear approximation.

The LM algorithm combines elements of both the steepest descent and Gauss-Newton methods. During training, the error at the output is computed by comparing the desired output vector (linear output) with the actual output vector (nonlinear output) resulting from the sensor's input (nonlinear output).

$$e_v = d_v - a_v \tag{2.2}$$

where e_m - Training Error in voltage, d_v - Desired output vector in volts and a_v - Actual output vector from sensor in volts. The sum square error(E_v) is calculated from the training error as follows.

$$E_v = \frac{1}{2}\sum_{p=1}^{p}\sum_{m=1}^{m} e_v^2 \tag{2.3}$$

The steepest descent algorithm uses the first-order derivative of the error function with respect to weight and can be called a gradient. Thus, the change in weight of the steepest descent algorithm is the function of the previous weight and the gradient (g). Unlike the steepest descent algorithm, Newton's method implies that all gradient components are functions of the weights, as follows.

$$\frac{\partial g}{\partial w} = \frac{\partial^2 E_v}{\partial w_i \, \partial w_j} \tag{2.4}$$

Consequently, the second-order derivatives of the total error function must be determined for each component of the gradient vector. The resulting matrix is called the Hessian matrix. However, the computation of the Hessian matrix is complex and can be simplified by introducing the Jacobian matrix, which represents the first-order partial derivatives of an error function. Thus, the algorithm LM is constructed using the Jacobian matrix and a combination coefficient μ. The weight change in each iteration using the LM algorithm is as follows.

$$w_{k+1} = w_k + H^{-1} J_k e_K \tag{2.5}$$

Thus, the convergence speed of the LM algorithm is stable and fast due to the introduction of the combination coefficient μ. It is challenging to determine the ideal number of hidden neurons, but a workable solution has been developed and is described in the paper [18].

2.3. Translinear circuits

The term "translinear" denotes the linear correlation between the drain current and transconductance in MOSFETs. Figure 1 showcases a circuit that possesses the ability to embody fundamental mathematical expressions by adhering to the translinear principle in both stacked and folded configurations [19]. According to the translinear principle of MOSFETs, assuming a zero-body effect

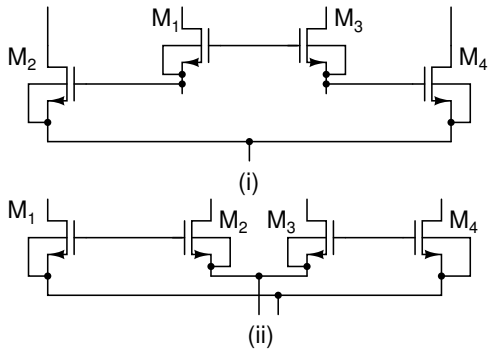

Figure 1. Translinear principle (i) Stacked loops (ii) Folded loops.

(connecting bulk of the NMOS to its source in a process with deep N well), the product of clockwise and counterclockwise currents remains constant. The MOSFET is dependent on the exponential current-voltage relationship of a circuit element. The ideal element follows the current relationship as follows.

$$I = I_S \times e^{\frac{V_{gs}}{\eta V_T}} \tag{2.6}$$

where I_S is the saturation current, V_{gs} is the gate-source voltage, V_{Th} is the threshold voltage, V_T is the thermal voltage, μ is the mobility of the electrons, C_{ox} is the oxide capacitance per unit area and n is the weak inversion slope factor. According to Kirchhoff's law applied to the loop, the sum of the voltages around the device, connected clockwise and counterclockwise respectively, is equal to zero.

$$\Sigma_{cw} V_{GS} = \Sigma_{ccw} V_{GS} \tag{2.7}$$

Because of the exponential characteristics as expressed in the above Eq 2.6, the translinear principle can be expressed as follows.

$$I_1 \times I_2 = I_3 \times I_4 \tag{2.8}$$

Eqs (2.7) and (2.8) enables us to realize simple mathematical operations such as multiplication and division using translinear or current mode circuits.

2.4. Field programmable array

A Field Programmable Array (FPGA) is a type of programmable logic device (PLD) that offers a high degree of flexibility and customization for digital circuit design. It consists of an array of configurable logic blocks interconnected by programmable interconnects. The logic blocks typically include lookup tables, registers, multiplexers and other digital components. The key feature of an FPA is its ability to be reconfigured or programmed by the user to implement specific digital functions or circuits. This programming is done using hardware description languages (HDLs) or graphical tools that allow designers to define the desired functionality and interconnections.

3. Results

In this study, translinear circuits are utilized to implement piecewise and neural regression models for sensor linearization. The chosen sensors for evaluation are T, K, N and J-type thermocouples and

an RTD (Pt-100). Table 1 presents the measurement range, full-scale error (FSE) and mean square error (MSE) of these sensors prior to linearization. To facilitate the translinear implementations, the sensor outputs were scaled within the range of 0-5μA.

Table 1. Details of chosen sensors.

Sensor	Range in °C	FSE BL%	MSE BL%
T-type	0-440	±5.50%	15.90
K-Type	0-1360	±2.51%	2.33
N-Type	0-1300	±3.49%	4.82
J-Type	0-1200	±2.42%	2.07
Pt-100	0-660	±2.71%	3.84

3.1. Implementation of piecewise regression model

The process of piecewise or segmented regression involves partitioning sensor data into distinct segments with predetermined breakpoints or nodes distributed uniformly. A function is then fitted to each segment to capture the underlying relationship. This study employs the 'R' programming language to identify the breakpoints and establish the piecewise regression model for aligning the sensor output with a straight line. 'R' serves as a statistical computation and analysis tool, enabling the creation of an optimized regression model for the sensor. Specifically, the "segmented function" in 'R' is utilized to identify the breakpoint within the sensor data and provide the corresponding fitted piecewise regression model for values above or below the breakpoint. This research uses translinear circuits to implement the fitted piecewise model. As depicted in Figure 2, the block diagram illustrates the integration of a multiplexer (MUX) to switch circuit operations based on the identified breakpoints.

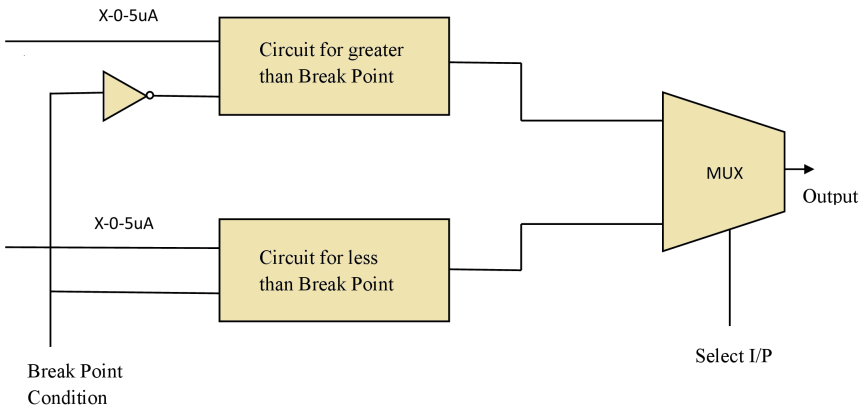

Figure 2. Block diagram of piecewise implementation.

3.2. Description of the circuit

3.2.1. Circuit for piecewise linearization for input less and greater than the Breakpoint

Figure 3 displays the comprehensive circuit diagram illustrating the translinear implementation of the piecewise model. The mathematical representation of the piecewise regression model for a sensor output (*'x'*) below the breakpoint is as follows.

$$y = \beta_0 + \beta_1 \times x \tag{3.1}$$

In this case, β_0 and β_1 represent the regression coefficients or slopes of the line segments between *'x'* = 0 and the breakpoint. Within the circuit, these regression coefficients, denoted as *'I_1'* and *'I_2'*, are combined with the sensor input *'x'*, as depicted in Figure 3. The mathematical operations necessary for inputs below the breakpoint are executed using the translinear principle. Translinear circuits, as current-mode circuits, adhere to the translinear principle effectively within the sub-threshold region, as outlined in reference [20]. The transistors in the circuit operate within the sub-threshold region, exhibiting a relationship between I_D and V_{GS} described by the following equation.

$$I_D = I_S \times e^{\frac{V_{gs}-V_{Th}}{\eta V_T}} \tag{3.2}$$

The saturation current I_S can be calculated as follows.

$$I_S = 2n\mu C_{ox}\frac{W}{L}{V_T}^2 \tag{3.3}$$

where V_{gs} is the gate-source voltage, V_{Th} is the threshold voltage and V_T is the thermo-electric voltage, μ is the electron mobility, C_{ox} is the oxide capacitance per unit area and n is the weak inversion slope factor. The output of the sensor 'x' is supplied to the multiplication circuit through a low voltage cascade current mirror (M_{32} to M_{44}). The supply voltage for the circuit is 2.5 V. Transistors M_{46}, M_{48}, M_{51}, and M_{53} perform multiplication with the regression coefficients of say 'I_1', while M_{45}, M_{49}, M_{50}, and M_{54} are native NMOS (NMOS with negative V_{th}) devices, which act as cascode devices and are necessary to reduce the mirror error caused by channel length modulation in translinear multiplication devices. Transistors M_{47} and M_{52} are employed to realize the current sources of 'I_1A' and 1μA. The implemented equation for linearizing the sensor input greater than breakpoint is as follows.

$$y = \beta_0 + \beta_1 \times k + (\beta_1 + \beta_2) \times (x - k) \tag{3.4}$$

Through the substitution of the determined coefficient values, the aforementioned equation can be simplified to reduce circuit complexity. As a result, the required calculation for implementation involves solely the product of the breakpoint and *'x'*, combined with a constant term. The multiplication operation is carried out by transistors M_{21}, M_{23}, M_{26}, and M_{28}. The error correction is achieved through the utilization of native NMOS devices, denoted by a bubble at the gates, represented by transistors M_{20}, M_{24}, M_{27}, and M_{29}. Transistors from M_7 to M_{19} are employed as low-voltage cascode current mirror.

3.3. Switching of circuits operation as per break points

This section describes the process of switching circuit operations based on whether the sensor input is below or above the breakpoints. The identified breakpoint, obtained through the use of the 'R'

language, is represented in the circuit as *'k'*, which falls within the microampere range and is controlled by transistors M_3 and M_4. The sensor input, denoted as *'x'*, is compared to the breakpoint *'k'* using transistors M_5 and M_6. The input of the inverter, formed by the combination of transistors M_1 and M_2, becomes either high or low depending on whether the current *'x'* exceeds or is below the current *'k'*. Consequently, when the input is high, the output of the inverter becomes low, and vice versa.

Furthermore, the output of the inverter serves the purpose of circuit selection through a multiplexer (MUX). The MUX is constructed using transmission gates spanning from M_{58} to M_{61}. A transmission gate, similar to a relay, operates as an electrical device based on CMOS technology. It consists of a parallel connection between nMOS and pMOS transistors, wherein the gate input of one transistor (C) is the complement of the gate input of the other transistor ($\bar{C}$). The inverter configuration involving transistors M_{56} and M_{57} facilitates the generation of states such as C and $\bar{C}$. Consequently, the output of the piecewise fitted polynomial circuits, representing the current flowing through the port named as I_{OUT}, is selected based on the states of C and $\bar{C}$.

The CADENCE/VIRUTOSO software tools are employed for the design and simulation of the circuit. The breakpoint in the output of a T-type thermocouple, which is 1.909, is detected by the 'R' programming language. The fitted regression model for a value less than 1.909 is shown below.

$$y = 0.03634 + 1.15548 \times (x) \tag{3.5}$$

Equations (3.6) and (3.7) give the regression model for more than the breakpoint at 1.909.

$$y = 0.03634 + (1.15548 \times 1.909) + x_1 \tag{3.6}$$

where x_1 is equal to

$$x_1 = 0.89994 \times (x - 1.909) \tag{3.7}$$

The W/L ratio of MOSFET's employed in the Figure 3 is as follows.
M_1, M_2 and M_{58} to $M_{61}$are 150n/280n
M_3, M_4 are $2\mu/4\mu$
M_5, M_6 are 5μ/900n
The W/L ratio MOSFET's employed for circuit less than and greater than breakpoints are employed as similar to Neural Network implementation as mentioned in the forthcoming section.

Table 2 illustrates the FSE of before and after linearization of the T-type thermocouple during the translinear implementation of the piecewise regression model. The linearization process yields a remarkable enhancement in linearity, with an FSE improvement of approximately ±1.38% compared to the calculated FSE of ±0.91%. Consequently, the piecewise translinear model achieves a significant boost in linearity, surpassing 75% improvement for the T-type thermocouple.

3.4. Implementation of neural regression model

The proposed scheme, depicted in Figure 4, illustrates the LM-based Artificial Neural Network (ANN) algorithm utilized for the linearization of the chosen sensors. To reduce the circuit's complexity, the network is constructed with only two hidden neurons, accompanied by an input and output neuron. The weights from the input neuron to the hidden neurons are denoted as W_1 and W_2 respectively, while the weights from the hidden neurons to the output neuron are represented as W_3 and W_4. In this study, a linear activation function is employed, ensuring that the neurons' output is directly proportional to

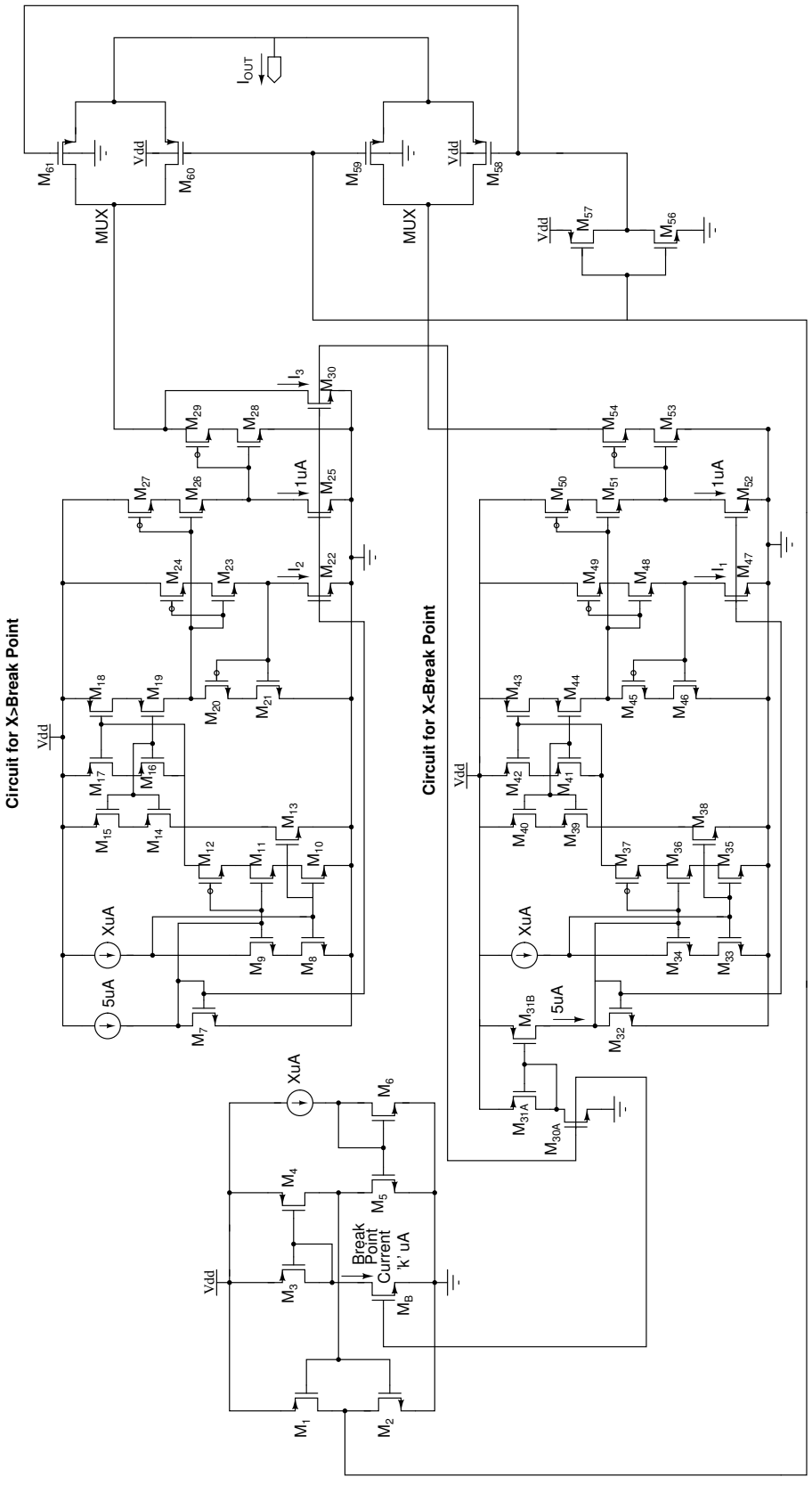

Figure 3. Translinear implementation of piecewise sensor linearization.

Table 2. Output and FSE before and after linearisation obtained for 'T' type thermocouple using translinear implementation of piecewise regression.

Temp °C	Thermo current (μA)	FSE BL (%)	Computed O/P (μA)	Computed FSE (%)	Simulated O/P (μA)	FSE AL (%)
0	0.0000	0.0000	0	0	0	0
40	0.3862	2.2767	0.4912	0.176	0.566	-1.34
80	0.8044	3.9115	0.972	0.56	1.069	-1.38
120	1.2524	4.9521	1.4924	0.152	1.558	-1.2
160	1.7270	5.4609	2.0451	-0.902	2.061	-1.2
200	2.2250	5.5002	2.5312	-0.624	2.566	-1.32
240	2.7448	5.1035	3.02	-0.4	3.012	-0.24
280	3.2841	4.3187	3.532	-0.64	3.457	0.86
320	3.8406	3.1890	4.036	-0.72	3.967	0.66
360	4.4131	1.7382	4.512	-0.24	4.47	0.6
400	5.0000	0.0000	5.0262	-0.524	5	0

the input. The subsequent steps are executed within the 'R' programming language to determine the appropriate weights and biases.

- The network is created and configured.
- The scaled output of the sensor is fed into the input neuron.
- The weights and biases are initialized.
- The network is trained with the target vector.
- The results are predicted for the given data set.

Table 3 and Figure 5 demonstrate the optimal weights and biases determined for linearizing the specified sensor with the least amount of trained error.

Table 3. Optimum weights and biases for the proposed neural network model.

Type	W_1	W_2	W_3	W_4	b_1	b_2	b_3
T-type	0.64436	1.63631	5.68518	2.01173	-2.21548	-0.70058	-1.19858
K-type	0.93204	0.52208	2.83208	8.18654	-0.20509	-2.66857	-1.78962
N-type	0.97949	0.55153	3.52674	6.76359	-0.09446	-2.64308	-2.08422
J-type	1.07738	0.6447	3.08238	5.63306	-0.79933	-3.01839	-1.17706
Pt-100	1.0289	0.60259	2.23411	6.74618	-0.74817	-2.71474	-1.1044

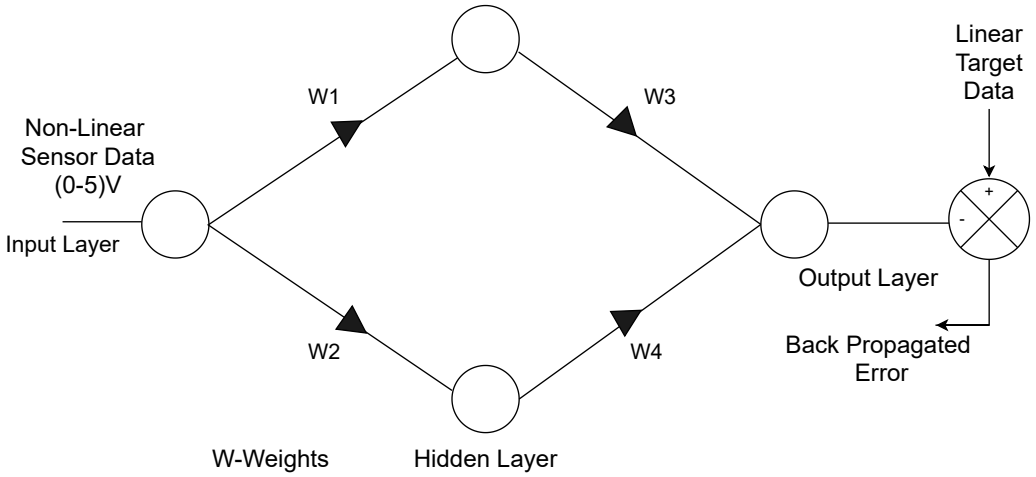

Figure 4. Proposed scheme of ANN model.

3.4.1. Description of the circuit

The detailed circuit diagram of the ANN model is presented in Figure 6. The output signal from the sensor, f(x), is first scaled down to a range of 0-5 μA and then fed into the circuit through the utilization of a cascode current mirror consisting of transistors M_2 to M_5. However, the standard cascode current mirror suffers from the drawback of larger input and output compliance voltage. To overcome this limitation, a low-voltage cascode current mirror, as depicted in Figure 6, is employed in this study to achieve the desired current-matching characteristics without a significant compliance voltage or voltage margin. In order to reduce the minimum allowable output voltage, the gate potential of transistor M_5 is decreased by an amount equal to the threshold voltage V_{Th}. To accomplish this, transistor M_1 is employed, with a current of 5 μA, to generate the necessary bias voltage for the cascode transistor. The width of M_1 is typically chosen to be 1/4th of the width of M_3. Equation 3.8 provides a description of the bias voltage generated by the cascode transistors.

$$V_B = V_{GS3} = V_{Th} + 2V_{OD} \tag{3.8}$$

Here, V_{OD} represents the overdrive voltage, which is calculated as $V_B - V_{Th}$. The same approach is applied to determine the current through the PMOS transistors (M_9 to M_{12}). The mirrored current flowing through transistors M_{3-4} is utilized to bias the current-sourcing PMOS transistors M_7 and M_8. The translinear principle, implemented using transistors M_{14}, M_{15}, M_{17} and M_{19}, facilitates the multiplication of the current from M_{11} by W_1. Error correction is performed through the use of native MOS transistors (M_{13}, M_{16}, M_{18}, and M_{20}). These transistors have a negative or close-to-zero threshold voltage, which helps reduce the difference in V_{ds} and thus ensures that the current replicates the input source. The output of the hidden neuron (y_1) is observed at the drain of transistor M_{20}, and it is combined with the bias current (b_1).

$$y_1 = f(x) \times W_1 + b_1 \tag{3.9}$$

Furthermore, the calculation of the output neuron is accomplished by copying the drain current from M_20 via M_{21} to M_{23}A. Since the activation function used in this study is a simple linear activation

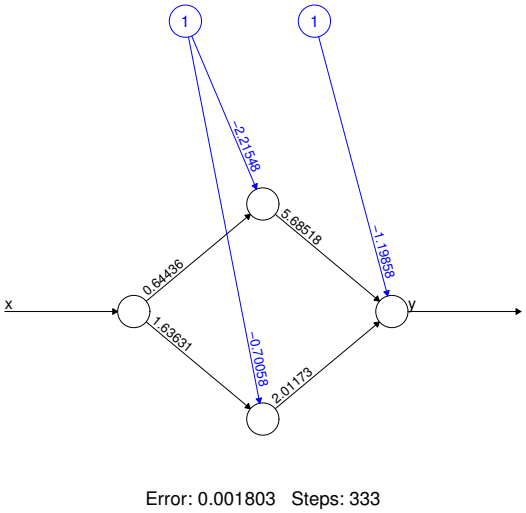

Figure 5. ANN model for T-type thermocouple.

function, the current of the PMOS mirror is directly multiplied by the weight W_3 using translinear multipliers (M_{25} to M_{30}). To reduce the error, the native NMOS devices marked with a bubble at the gates (M_{24}, M_{27}, M_{29}, M_{31}) serve as cascode devices. The circuit employed in this work for multiplying the currents(i.e f(x) x W1) can also able carry out the division of two currents by replacing the 1μ with a divisible value. The circuit utilizes transistors, specifically M_{15A}, $M-17A$, M_{19A}, M_{26A} and M_{28A}, to realize the current sources responsible for representing weights and biases with respect to the ratio of width to length of the copying transistor(M_1).

$$y_2 = y_1 \times W_3 \tag{3.10}$$

Similarly, the calculation of the second hidden neuron and its output neuron computation is performed with the corresponding weight (not shown in the figure) and added to the previous result (y_2). The transistors performing the translinear multiplication/division operate in the sub-threshold region as expressed in the equation.

The ratio of W/L of MOSFET's employed in Figure 6 are as follows.
M_1, M_7, M_8 are $2\mu/4\mu$
M_3, M_4 are $2\mu/1.25\mu$
M_2, M_5 are $2.5\mu/300$n
M_9, M_11 are $9\mu/1\mu$
M_9, M_11 are $1\mu/1\mu$
M_14, M_19, M_25, M_38, are $30\mu/600$n
M_15, M_17 are $30\mu/600$n
The circuit design and simulation of the ANN Model for the T-type thermocouple were performed using the CADENCE/VIRTUOSO tools. The results of the translinear implementation are presented in Table 4, covering a temperature range of 0°C to 440°C. The maximum Full-Scale Error (FSE) achieved during the implementation is 1.16%, significantly reduced from the initial value of 5.5% before linearization. Consequently, the linearity improvement for the T-type thermocouple amounts to nearly 80% after linearization.

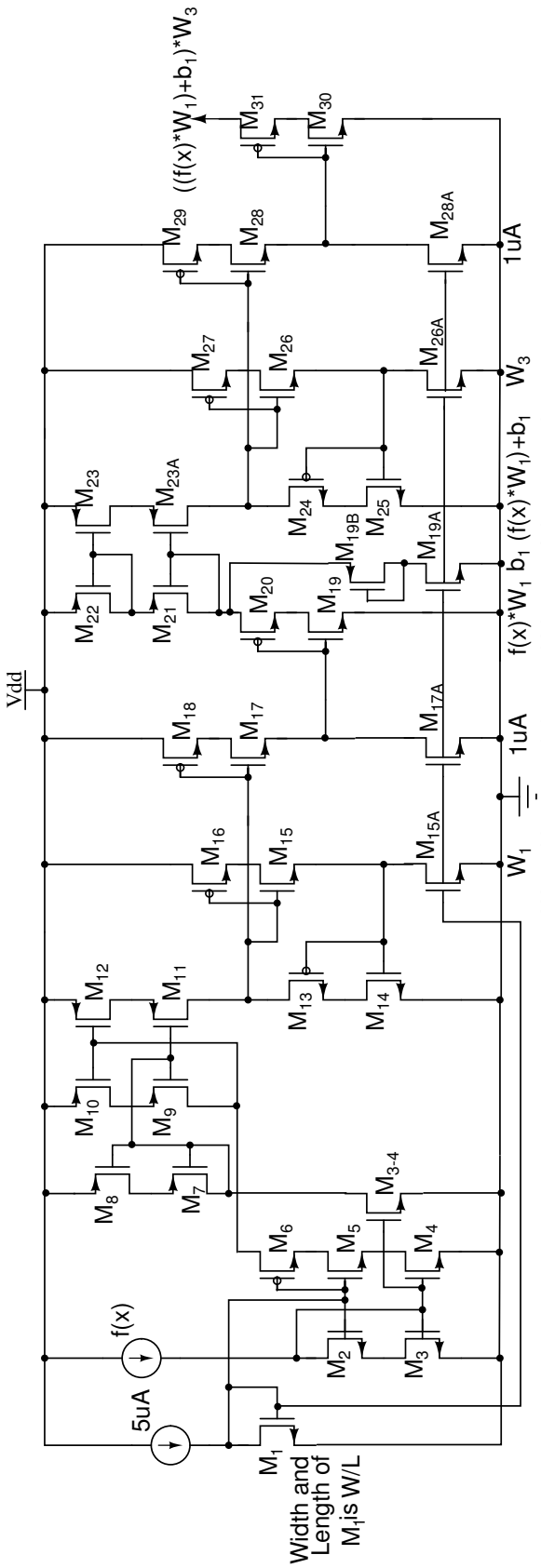

Figure 6. Translinear implementation of neural network algorithm.

Table 4. Output and FSE before and after linearisation obtained for 'T' type thermocouple using translinear implementation of ANN algorithm.

Temp °C	Thermo current (μA)	FSE BL (%)	Computed O/P (μA)	Computed FSE (%)	Simulated O/P (μA)	FSE AL (%)
0	0.0000	0.0000	0.02792	-0.55841	0	0
40	0.3862	2.2767	0.47064	0.58715	0.4981	-0.036
80	0.8044	3.9115	0.98777	0.24443	0.9911	-0.176
120	1.2524	4.9521	1.51556	-0.31136	1.5331	0.662
160	1.7270	5.4609	2.01555	-0.31119	2.0446	0.89
200	2.2250	5.5002	2.49695	0.06091	2.5497	0.994
240	2.7448	5.1035	2.98660	0.26794	3.058	1.16
280	3.2841	4.3187	3.49606	0.07869	3.5413	0.826
320	3.8406	3.1890	4.014647	-0.29294	4.0321	0.642
360	4.4131	1.7382	4.51734	-0.34681	4.5291	0.582
400	5.0000	0.0000	4.97529	0.49419	4.9913	-0.174

3.5. FPGA implementation

In this study, to enable a comparison between analog and digital domain results, the implementation of ANN and Piecewise models was also carried out on an FPGA. In FPGA devices, arithmetic operations can be executed using floating-point or fixed-point arithmetic. In this study, fixed-point arithmetic is employed, utilizing varying bit lengths for the input and output. The input thermo-EMF and linearizing parameters, such as weights, biases, and polynomial coefficients, are assigned bit lengths of seven and eight bits for the integer and fractional parts respectively. For enhanced accuracy and precision, the output bit length is set between 8 to 16 bits. To implement the function of ANN and piecewise models, an algorithm is devised that encompasses various mathematical operations. The binary output generated by Xilinx-Verilog is loaded into the FPGA device for execution. Table 6 summarises the FPGA-based ANN and piecewise linearization of all the chosen sensors. theoretically computed FSE is 0.171

4. Discussion

The performance evaluation of the translinear implementation for both the piecewise fitted regression and ANN models applied to thermocouples and RTD are illustrated in Figure 7–11, accompanied by the corresponding data presented in Table 5. The outcomes of our proposed implementation are compared with the results obtained by other researchers for comprehensive analysis and comparison.

The piecewise regression model divides the sensor data into segments and fits a linear regression within each segment. In analyzing the linearization results of the selected sensors, we can assess the

Table 5. Output and FSE before and after linearisation obtained for the chosen sensors using translinear implementation of PW and ANN models.

SI.No	Sensor	FSE BL	FSE AL PW	FSE AL NN
1	T-Type	5.50%	1.38%	1.16%
2	K-Type	2.41%	1.26%	0.98%
3	N-Type	3.47%	3.00%	1.42%
4	J-Type	2.34%	0.76%	0.95%
5	Pt-100	2.68%	0.59%	0.56%

Table 6. Output and FSE before and after linearisation obtained for the chosen sensors using FPGA implementation of PW and ANN models.

SI.No	Sensor	FSE BL	FSE AL PW	FSE AL NN
1	T-Type	5.50%	0.724%	0.561%
2	K-Type	2.41%	0.941%	0.374%
3	N-Type	3.47%	1.931%	0.639%
4	J-Type	2.34%	0.534%	0.597%
5	Pt-100	2.68%	0.452%	0.523%

proximity of each Thermo EMF data point to the corresponding temperature value. For the T-type thermocouple and the Pt-100, the data points (representing Thermo EMF values over the temperature range) are widely spread apart, allowing the piecewise method to generate an excellent regression model. Consequently, the translinear implementation achieves a percentage linearity of approximately 75% for the T-type thermocouple and 85% for the Pt-100. These sensors exhibit consistent exponential characteristics across their entire temperature range.

In contrast, other sensors such as K, N and J-type thermocouples have data points that are closely clustered together and exhibit different trends within their measurement range. As a result, the percent linearity improvement achieved for these sensors is lower: 45% for the K-type thermocouple, 15% for the N-type thermocouple and 55% for the J-type thermocouple. It becomes evident that the piecewise regression model is less effective in capturing the nonlinearity of these sensors. To enhance the linearity of such sensors, employing more breakpoints becomes necessary. However, increasing the number of breakpoints or equations also leads to a rise in circuit complexity.

On the contrary, the neural network proves to be effective in addressing nonlinearity issues, as it can implicitly capture the nonlinear relationships between variables with minimal training. Implementing the translinear approach for the T-type thermocouple results in an impressive 80% improvement in linearity compared to the desired predicted output of the neural network model, which stands at 90%. Given the exponential nature of the T-type thermocouple's ideal properties, the network is able to train efficiently across its entire range. In contrast, the characteristics of temperature and thermoelectric voltage of the K-type thermocouple demonstrate good linearity at lower temperatures but deviate from a straight line at higher temperatures. The problem of overfitting becomes more prevalent in the low-temperature range compared to the high-temperature range. Thus during the simulation, the linearity

of the K-type thermocouple is enhanced only by approximately 61%, while the theoretically predicted FSE improvement stands at 79%.

The linearity improvement resulting from the translinear implementation of the N and J-type thermocouples is consistent, as both thermocouples exhibit persistent deviations from a straight line and lack exponential characteristics. During the simulation, the linearity of the N and J-type thermocouples improves by approximately 60% compared to the theoretically expected FSE of 70% and 75%, respectively.

In the case of the Pt-100, despite its ideal features often deviating from a straight line, the LM algorithm successfully identifies the optimal model to accurately fit these characteristics. As a result, the translinear implementation achieves a remarkable linearity improvement of about 82%, surpassing the theoretically predicted outcome of 90%.

According to Table 6, the FPGA-based linearization demonstrates superior suppression of non-linearity compared to the translinear circuit. However, the main sources of error in the FPGA implementation are associated with bit errors, which can be mitigated by increasing the bit length. It is important to note that the FPGA-based approach has certain drawbacks, such as limited response speed, quantization errors, and higher power consumption.

The FSE accuracy is affected in the MOSFET-based translinear implementation because the MOSFET translinear principle is not well-suited for mixed transistor loops. As a result, the matching of N and P devices is impacted by scaling through the device's Width and Length. The weak inversion region in which the MOSFET operates poses a challenge to achieving linearity and contributes to the high error rate observed in the translinear implementation. Additionally, the MOSFET-based current mirrors utilized in the circuit, which serve to replicate current from one section to another, introduce their own sources of error. However, the inherent correction mechanisms and the implementation of a low-voltage cascode arrangement effectively mitigate the inaccuracies arising from the current mirrors, resulting in reduced error. The performance of the proposed implementation is compared with the existing techniques in Table 7.

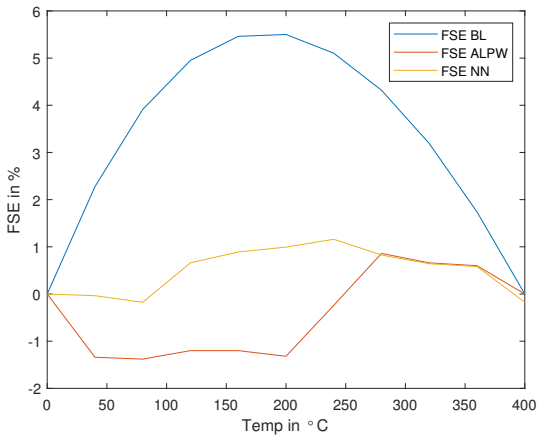

Figure 7. Percentage FSE of proposed PW and neural model of translinear implementations for 'T' type thermocouple.

Table 7. Comparison between proposed implementation and existing techniques.

Author and method adopted	**Chosen Sensor**	**Improvement in the linearity**	**Remarks**
Srinivasan et al. Data driven method	J-Type & K-Type	0.12% FSE 0.41% FSE	Efficient identification of linear model with computational complexity
Zivanovi et al. Two stage segment linearization	T-,J-,K- and N-Type	0.2 deg Celcius	Implementing through Microcontroller, achieving good linearity poses challenges in terms of memory requirement, speed of response and power consumption
Anandanatarajan et al. Polynomial non-linear regression technique	K-Type	0.02%	Excellent improvement in the linearity at the cost of complex implementation
Sundararajan et al. Translinear implementation of evolutionary optimized algorithm	T-, J-, K- and N-Type	74%, 42%, 47% and 45% respectively.	A fair amount of improvement in the linearity using analog domain
Proposed implementation of Neural Network based Translinear Circuit	T-, J-, K- and N-Type	80%, 60%, 60% and 60% respectively	1. Substantial improvement in the linearity as compared to the translinear implementation of evolutionary optimized function and other methods. 2. Demonstrate exceptional performance in terms of power consumption and speed of response.

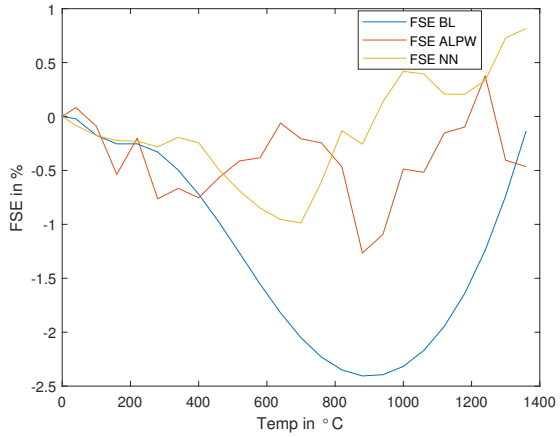

Figure 8. Percentage FSE of proposed PW and neural model of translinear implementations for 'K' type thermocouple.

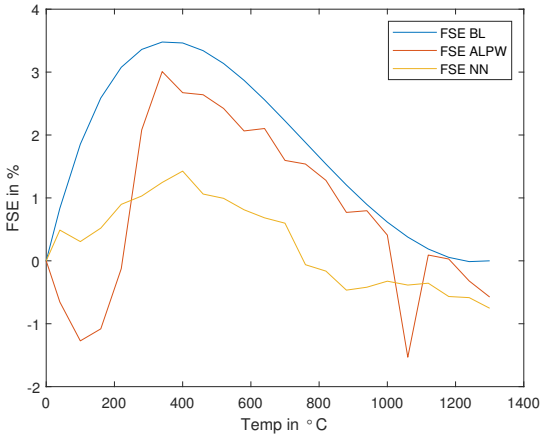

Figure 9. Percentage FSE of proposed PW and neural model of translinear implementations for 'N' type thermocouple.

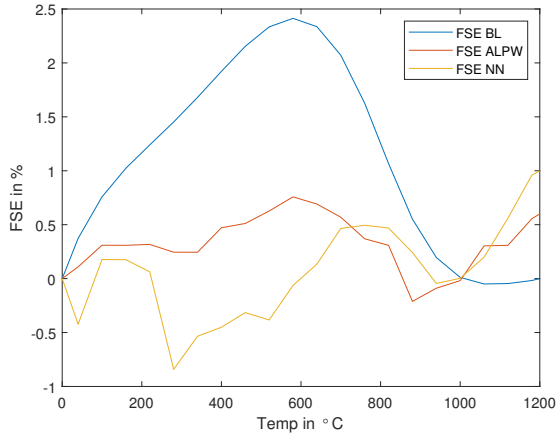

Figure 10. Percentage FSE of proposed PW and neural model of translinear implementations for 'J' type thermocouple.

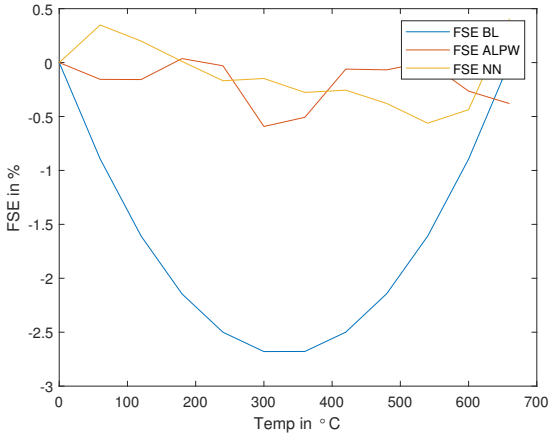

Figure 11. Percentage FSE of proposed PW and neural model of translinear implementations for 'Pt-100' type thermocouple.

5. Conclusions

The proposed implementation of translinear circuits for both the piecewise regression and artificial neural network (ANN) regression models provides a practical approach for enhancing the linearity of transducers in analog mode. A comparison is made between the results obtained from this implementation and those of previous studies. In terms of reducing non-linearity errors in the selected sensors, the ANN-based translinear circuit outperforms the piecewise regression-based circuit. The performance of current mode circuits based on the piecewise regression model is hindered by challenges in accurately detecting and identifying appropriate breakpoints. Increasing the number of breakpoints can improve linearity for sensors with diverse trends throughout their operating range, but it also leads to increased circuit complexity.

On the other hand, the neural network technique, with a limited number of neurons, excels in minimizing non-linearity errors in the sensors. Optimized weights are obtained through offline training using the Levenberg-Marquardt (LM) technique to achieve the lowest relative error. While increasing the number of neurons can enhance linearity, it also increases circuit complexity. The issue of overfitting negatively impacts the results for K, N and J type thermocouples.

At the circuit level, errors arise from variations in threshold voltage and aspect ratio of transistors, as well as assumptions of exponential relationships between drain current and gate-to-source voltage. Despite these challenges, the MOSFET-based translinear circuit implementation offers advantages over previous works in terms of response time and power consumption. As compared to FPGA devices(30μ), the proposed translinear implementation consumes significantly lower power, approximately 1μW. To further improve linearity, the MOSFET-based translinear circuit can be replaced with a BJT, which follows the exponential law across a wide current range and exhibits excellent matching characteristics. The advantages in power consumption and response speed position analog computation as superior to digital computation for edge computing applications.

Use of AI tools declaration

The authors declare they have not used Artificial Intelligence (AI) tools in the creation of this article.

Acknowledgments

The authors would like to thank the Federal Institute of Science and Technology and Cochin University for providing the necessary resources and the conducive environment to carry out this research work.

Conflict of interest

The authors declare that there is no conflict of interest regarding the publication of this paper

References

1. Murmu A, Bhattacharyya B, Munshi S (2018) A synergy of voltage-to-frequency converter and continued-fraction algorithm for processing thermocouple signals. *Measurement* 116: 514–522. https://doi.org/10.1016/j.measurement.2017.11.047
2. Ximin L (2010) A linear thermocouple temperature meter based on inverse reference function. *International Conference on Intelligent Computation Technology and Automation* 1: 138–143. https://doi.org/10.1109/ICICTA.2010.284
3. Mukherjee A, Sarkar D, Sen A, Dey D, Munshi S (2013) An analog signal conditioning circuit for thermocouple temperature sensor employing thermistor for cold junction compensation. *International conference on control, automation, robotics and embedded systems*, 1–5. https://doi.org/10.1109/CARE.2013.6733711
4. Mondal N, Abudhahir A, Jana SK, Munshi S, Bhattacharya DP (2009) A log amplifier based linearization scheme for thermocouples. *Sensors & Transducers* 100: 1.
5. Srinivasan K, Sarawade PD (2019) An included angle-based multilinear model technique for thermocouple linearization. *IEEE Transactions on Instrumentation and Measurement* 69: 4412–4424. https://doi.org/10.1109/TIM.2019.2947951
6. Wen D, Qing L, Qiang L (2007) Calibration system for thermocouple application based on technology of virtual instrument and neural network. *8th International Conference on Electronic Measurement and Instruments,* 1–268. https://doi.org/10.1109/ICEMI.2007.4350439
7. Sundararajan S, Kottarthil Naduvil M, Abudhahir A, Karuna KG, Noble G (2022) Synthesis and study of evolutionary optimised sensor linearisation with translinear & FPGA circuits. *International Journal of Electronics* 109: 699–720. https://doi.org/10.1080/00207217.2021.1941287
8. Radetić R, Pavlov-Kagadejev M, Milivojević N (2015) The analog linearization of Pt100 working characteristic. *Serbian Journal of Electrical Engineering* 12: 345–357. https://doi.org/10.2298/SJEE1503345R

9. Hotra O, Boyko O (2015) Analogue linearization of transfer function of resistive temperature transducers. *In Photonics Applications in Astronomy, Communications, Industry, and High-Energy Physics Experiments* 9662: 1230–1237. https://doi.org/10.1117/12.2205449
10. Abudhahir A, Baskar S (2008) Analogue linearization of transfer function of resistive temperature transducers. *Measurement Science and Technology* 19: 045103. https://doi.org/10.1088/0957-0233/19/4/045103
11. Ghaly SMA (2019) LabVIEW based implementation of resistive temperature detector linearization techniques. *Engineering, Technology & Applied Science Research* 9: 4530–4533. https://doi.org/10.48084/etasr.2894
12. Živanović D, Simić M (2021) Two-stage segment linearization as part of the thermocouple measurement chain. *Measurement and Control* 54: 141–151. https://doi.org/10.1177/0020294020986833
13. Anandanatarajan R, Mangalanathan U, Gandhi U (2022) Linearization of temperature sensors (K-type thermocouple) using polynomial non-linear regression technique and an IoT-based data logger interface. *Experimental Techniques,* 1–10. https://doi.org/10.1007/s40799-022-00599-w
14. Phadnis, MG (2020) Real time linearization of sensor response using a novel polynomial estimation method. *IEEE Instrumentation & Measurement Magazine* 23: 73–78. https://doi.org/10.1109/MIM.2020.8979528
15. Khan SA, Shahani DT, Agarwala AK (2003) Sensor calibration and compensation using artificial neural network. *ISA transactions* 42: 337–352. https://doi.org/10.1016/S0019-0578(07)60138-4
16. Sundararajan S, Kottarthil Naduvil M, Abudhahir A, Karuna KG, Noble G (2022) Synthesis and study of evolutionary optimised sensor linearisation with translinear & FPGA circuits. *International Journal of Electronics* 109: 699–720. https://doi.org/10.1080/00207217.2021.1941287
17. Van Ooyen A, Nienhuis B (1992) Improving the convergence of the back-propagation algorithm. *Neural networks* 5: 465–471. https://doi.org/10.1016/0893-6080(92)90008-7
18. Vujičić T, Matijevi T, Ljucović J, Balota A, Ševarac Z (2016) Comparative analysis of methods for determining number of hidden neurons in artificial neural network. *In Central european conference on information and intelligent systems* 219.
19. Shaterian M, Twigg CM, Azhari J (2013) An MTL-based configurable block for current-mode nonlinear analog computation. *IEEE Transactions on Circuits and Systems II: Express Briefs* 60: 587–591. https://doi.org/10.1109/TCSII.2013.2268660
20. Serrano-Gotarredona T, Linares-Barranco B, Andreou AG (1999) A general translinear principle for subthreshold MOS transistors. *IEEE transactions on circuits and systems I: fundamental theory and applications* 46: 607–616. https://doi.org/10.1109/81.762926